Proceedings of the IASS Annual Symposium 2025
"The living past as a source of innovation"
27 October– 31 October 2025, México City, México>
<Juan Gerardo Oliva, Juan Ignacio del Cueto, Elisa Drago (eds.)

Realisation of Prefabricated Geodesic Dome

Corresponding AUTHOR*, Szymon M. Jankowski

*Wroclaw University of Science and Technology
Boleslawa Prusa 53-55, Wroclaw 53-100, Poland
szymon.jankowski@pwr.edu.pl

Abstract

The presentation covers the successful assembly of an 11-meter geodesic dome prototype made from thin-walled glass fiber-reinforced concrete (GFRC) panels. This full-scale model validated panel design and structural assembly methods. The study details fabrication stages, focusing on structural rigidity and manufacturing tolerances. Design and technology choices impacted final assembly and validation. Key challenges included maintaining angular precision between panels, testing a proprietary connection system, and examining how the installation sequence affected overall stiffness. The research also assessed custom tools such as an adjustable strut positioning system and specialized scaffolding for alignment. Repeated assembly cycles were analyzed for their impact on joint flexibility and progressive structural stiffening. Despite technical challenges, the prototype showed adequate stiffness and damping, with deviations within acceptable limits. Located at the Faculty of Architecture at Wrocław University of Science and Technology, the dome will serve in long-term studies on durability and usability under extended operational conditions.

Keywords: prefabricated structure realisation, geodesic dome, assembling process, repetitive assembly and disassembly

1. Introduction

Fullerian geodesic domes, widely popularized, derive from the concept of "doing more with less," frequently referenced in [1]. As geometric approximations of a sphere using flat-panelized surfaces, they present numerous challenges in conceptual design, extensively discussed in [2]. The form-finding process in Fuller-type domes involves balancing geometric fidelity, the number of components, and formal variation, as previously analyzed in [3]. Utilizing a single triangular panel shape limits diversity to scale alone, yet necessitates a high number of custom joints, which significantly reduces the potential for prefabrication [4]. Subsequent design phases introduce additional complexity in detailing, including bearing interfaces and joint design, as explored in [5]. The joining of components becomes a non-trivial aspect, requiring preemptive strategies for sequencing, assembly logic, and tolerances—thus partially compromising the idealized behavior of the spatial structure.

To date, most implementations of the so-called "Fullerdome" typology have relied on bar-node systems, where lightweight openwork structures carry only axial forces. Iconic examples such as the Biosphere and the U.S. Pavilion at Expo represent the early ideological and structural interpretations of the Fullerian dome concept, detailed in [6]. Their fabrication was based on high-strength steel members connected via welding and mechanical joints. The outer layers in all these structures were limited to protective skins, not contributing structurally to the load distribution or stiffness. These domes could be entirely constructed using Fuller's own thin-walled tubular steel systems. Conversely, the Carbondale Dome represents a more complex evolution, introducing depth to the structural components, which necessitated higher fabrication precision and the development of linear panel-to-panel joints [7]. From both a modeling and fabrication perspective, these systems addressed new challenges by introducing innovative solutions at each stage of development.

This study presents the assembly process of a geodesic dome structure entirely fabricated from GRC (Glassfibre Reinforced Concrete)—a material historically used in construction [8], but only recently applied to diversified forms such as thin-shell panels. The author was directly involved in the process, developing a coded identification system, panel assembly sequence, and supervising on-site execution. The dome realization was part of a funded research project led by DSc. Assoc. Prof. Waldemar Bober, at the Faculty of Architecture, Wrocław University of Science and Technology. The resulting structure stands out in its fabrication logic, design methodology, and the feedback-driven iteration of both primary and emergent solutions during the modeling and construction phases.

The dome was built using double-layer GRC panels made of high-strength fine concrete, joined with steel frame inserts. The structure was tri-layered: each concrete panel (top and bottom skins) included three steel C-channels embedded along its edge thickenings, forming the inter-panel jointing system. An 18 cm cavity between the skins was left for insulation or service routing, resulting in two 2 cm concrete shells acting as the structural layers transferring stress across connections. The dome model has a diameter of 10 meters and an internal surface area of 74.5 square meters. It is made up of 105 panels, and the central point is located at a height of 1.7 m over base level. Overal height of dome closes in 6,72m. The geometry of the dome is based on a regular icosahedron. The reference sphere points precisely align with the virtual intersection nodal points at the corners. Due to the use of the icosahedron form, the dome had to be panelized using three types of triangular structural modules. Each panel reached a total thickness of 20 cm, with side lengths ranging from 152 cm to 181 cm. All three panel types were isosceles triangles of different sizes but with uniformed slope angle of edge borders. The dimensions of the steel inserts determined the use of plate-like connections, which enhanced stiffness and ensured more uniform load transfer across the dome's surface. The nodal zones, by contrast, remained completely unloaded and inactive in structural force distribution. Each node accommodated the convergence of five or six panels. Due to inherent requirements of geodesic construction, three different panel sizes were developed, arranged in a 9-panel repetitive module across the dome. This pattern presented further in papers produced a scaled-up rounded triangular motif repeated over the entire surface. The dome was mounted on custom continuous base elements cast as monolithic supports with embedded profiles complementary to those used in the panels. A triangular entrance opening was formed on the front elevation using a welded steel frame equal in size to four panels. Its primary function was to reinforce the model's global stiffness.[2]

2. Assembly preparation

The construction phase was preceded by the prefabrication of the dome's structural components. The model consists of 105 prefabricated elements made of glass-fiber reinforced concrete (GRC). The inherent geometry of the geodesic dome required differentiated panel shapes, although consistent joint angles were maintained across all elements to simplify the manufacturing process. This configuration

Figure 1: Molds and the process of their use for manufacturing GRC panels.

necessitated three distinct panel types to preserve the dome's overall geometry. The concrete mix was selected based on the required casting precision and the stiffness necessary for the panels to act structurally. The upper panels were cast in specially designed steel molds as shown in figure 1, incorporating embedded steel angle profiles with a tongue-and-groove assembly system. The dispersed glass fibers were mixed directly into the fresh concrete to ensure a homogeneous reinforcement distribution throughout the panel mass. The steel angles served as stiffeners and load-transferring components between adjacent panels. Given the dome's load regime—predominantly compressive—the steel profiles were designed to engage in diaphragm action, as confirmed by both preliminary numerical simulations and subsequent experimental testing.

Once the upper panel concrete had set, the lower panels were cast separately, maintaining precise chamfer angles and embedding the previously cast steel angles that extended from the upper elements. As a result, each component became a hybrid composite of concrete, fiberglass, and steel, fully ready for integration into the dome's spatial structure. During prefabrication, several production challenges emerged—most notably, the fragility of the panel corners as in figure 2. The acute angles of all triangular panels were prone to chipping, necessitating the introduction of minimal edge chamfers on all sides. Additionally, inconsistencies were observed in the interface zones between the steel angles and the concrete mass. Poor concrete compaction around the steel profiles led to insufficient embedding. Given that the diaphragm-like behavior relies on forces being transferred parallel to the anchorage axis along the C-profile flanges, numerical analysis indicated that anchorage performance was critical. Insufficient embedment was manifested through exposed glass fibers and material spalling at short edge zones of the panels. These defects resulted in debonding between steel and concrete, as well as water infiltration into the panel joints. Edge irregularities—visible in early series photographs—revealed inadequate concrete cover and uneven reinforcement behavior near panel margins, leading to accelerated degradation. Refinements in the concrete mix and improved vibration compaction during casting ultimately mitigated these defects and enhanced panel performance.

Figure 2: Inaccuracy in steel-to-concrete connections and joint misalignment causing non-shear behavior of the structure.

The diaphragm-based connection system, as opposed to traditional node-based assembly, required rigorous testing of the alignment tolerance between elements. Any angular misalignment between adjacent panels induced out-of-plane bending at the joints, leading to stress redistribution and a departure from purely compressive load paths. Experimental testing determined the maximum angular deviation tolerance to be 12 mm of edge misalignment (measured through panel thickness) between joined panels at a given dome level prior to loading upper segments. The initial design assumptions required maintaining inaccuracies below 2 angular degrees, which translates to a maximum gap between panels of 15 mm. This means that the minimum criterion has been met; however, the inaccuracy will affect the load-bearing capacity and the structural behavior of the model.

2.1. Dome bases

The construction of the geodesic dome began with the preparation of the surface beneath the base panels shown in figure 3. A 60 cm wide strip around the foundation perimeter was leveled, followed by the establishment of reference points for precise alignment of the base elements. Measurements were conducted using a laser gyroscope and distance meter, achieving an accuracy of ±3 mm. A leveling procedure was also carried out beneath the central support platform, which was required for assembling the upper dome segments. Due to its positioning in relation to the dome's focal point, this pedestal was installed at a height of 18 cm above the base panel level. Base elements were aligned based on reference coordinates, with distances continuously calculated from the (0,0) origin point. These base panels did not feature mechanical connectors, allowing them to be freely repositioned during the leveling and alignment phase. The layout progressed in a circular pattern, starting at the designated entrance location. Once all base panels were in place, they were temporarily braced to prevent movement during the installation of higher dome segments. The precise referencing allowed for accurate positioning of the final base element. It is estimated that positional accuracy could be reduced to 10 mm without compromising the structural assembly or overall dome behavior.

Figure 3: Diagram of base module arrangement and the research model implementation process

Due to their significant weight, base panels required continuous use of a lifting device. Although anchoring was theoretically possible via pre-formed anchor holes, the closed-ring nature of the dome's geometry resulted in zero net horizontal reactions, eliminating the need for permanent anchoring. Temporary anchoring, however, was applied to the first three panel layers due to their initial outward tilt; since the dome consists of 64% of a full spherical shell, the first rows of panels extend outward from the base. Temporary anchoring was essential to resist overturning moments during early stages of the build. After positioning the base components, alignment was re-verified. Three panels required minor correction of a single reference point due to minor production inaccuracies. The use of a more conventional concrete mix caused slight surface roughness and minor inter-panel gaps; however, this did not affect the angular or positional tolerances required for assembly.

3. Panels assembly

The dome consists of seven levels of prefabricated panels, arranged such that the focal point of the geometry is located at the interface between the first and second tiers. This layout results in a slight outward inclination of all panels, requiring careful planning of the assembly sequence. The first two levels do not generate significant horizontal forces and therefore do not require temporary support until the self-stabilizing geometry of the dome engages. During experimental testing, five types of joints were evaluated, with the final selection based on minimal flexibility and the ability to engage and disengage the connection without direct access to internal fasteners. Despite the focus on rigidity, a slight, controlled flexibility in the joint design proved beneficial during assembly. The theoretical precision required to ensure pure membrane (in-plane) behavior in the structure is exceptionally high; however, allowing for minor elastic adaptation at the steel-to-steel contact zones increased the tolerance margin during panel fitting. To avoid overloading connections and to limit changes in the direction of bending moments at panel joints, a precise assembly sequence had to be developed. This ensured that the partially built structure remained within safe working conditions, with loads appropriately distributed throughout the dome during the step-by-step erection process.

3.1. First level assembly

Assembly of the dome structure began at the entrance opening, initiating with the two bottom panels on the left and right, numbered 1 through 4 as in figure 4. Gradually, the first level of the dome was completed. Every two bottom panels required a third, upper panel to be locked in place, progressively closing the structural ring. This sequential interlocking approach minimized deformation during assembly and maintained high geometric precision. The components were lifted using a mobile crane

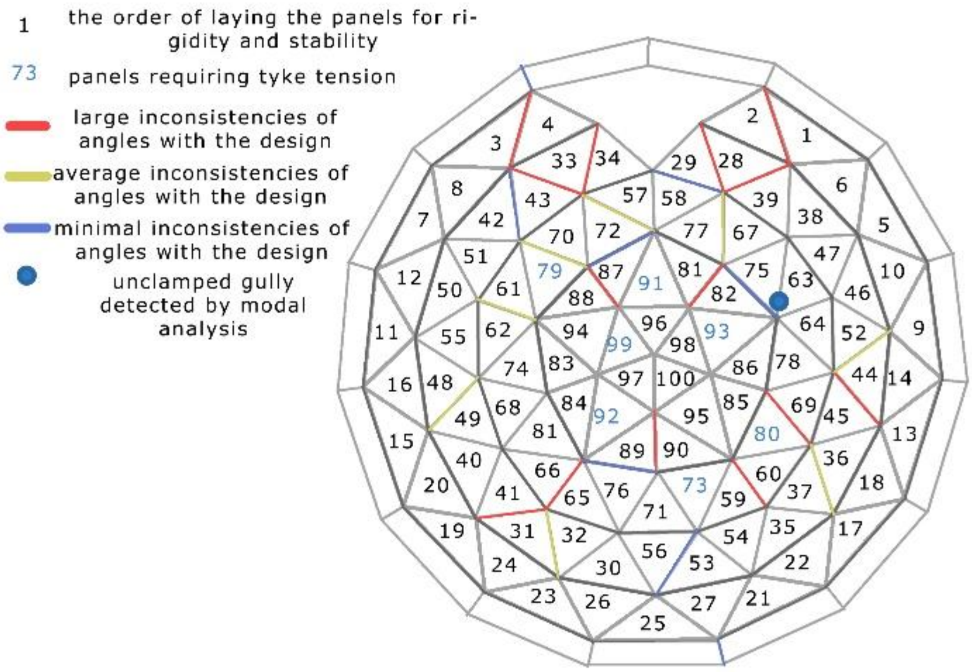

Figure 4: Sequence of panel assembly with mapped deviations in executed joint connections

and positioned manually. For the first two levels, panels could be transported in a vertical orientation, requiring only proper rotational alignment during placement. For the upper tiers, however, a custom positioning frame was employed—a steel rig equipped with a tilting platform adjustable in 24 discrete inclination settings. The desired angle was manually set, the panel placed on the platform, and then secured at the correct tilt with rigging lines before being hoisted into position. This method significantly reduced the need for angle and alignment corrections during placement and ensured accurate seating in the connector slots. The interlocking mechanism did not require deflecting neighboring panels, evidencing a high degree of fabrication precision. Self-supporting structural behavior emerged starting from the placement of panels 10 and 12. After each installation sequence, deformation measurements were taken. The vertical displacements of the inner panel vertices were compared to the digital reference model, with observed deflections ranging from 3.2 cm to 0.2 cm.

The final panel of each level required slight manual adjustment—neighboring panels had to be displaced outward by 3 cm on each side to accommodate the final fit. These adjustments remained within the permissible elasticity of the connection system. The repeated deflection measurements enabled the mapping of bending moment direction reversals. Analysis of this data showed 12 temporary shifts in the bending direction of individual panels, increasing the cumulative compliance in connections. This justified additional tests on alternative assembly sequences. Among nine tested strategies, two alternatives for the base layer were modeled and analyzed. However, they yielded inferior results, with 17 and 32 moment direction changes respectively.

Once the full level was assembled, parallelism of the joints was verified using feeler gauges. One internal connection exceeded the 2 mm tolerance limit. Prior to correction, non-contact zones in the exterior steel brackets were identified and assessed for complementarity with the internal misalignment. Recognizing such complementarity is essential for selecting the correction method, which involved applying rotational forces at selected panels. The adjacent panels on the exterior side of the misalignment were temporarily stiffened, while neighboring interior panels were manually pushed outward. This deliberate shifting of planes within the elastic limits of the connections eliminated the misalignment. The entire panel ring subsequently exhibited full membrane behavior as designed. Final verification of key vertex reference points showed deviation within ±3 mm of the digital model.

3.2.Second panels levels

As the assembly progressed to higher levels, the inclination of the panels increased, inducing greater bending forces in the elements acting in a cantilevered manner during installation. At the second level, assembly inaccuracies were significantly reduced due to the stiffening effect of the previously installed lower tier. Each sequential installation of three interlocking elements caused smaller global deformations or further enhanced the overall rigidity of the structure. With the completion of the second tier, the entrance opening was fully enclosed. No angular corrections were required at this stage; however, the last two modules necessitated slight outward deflection of adjacent panels. Once in place, this induced a beneficial pre-stressing effect due to the resulting structural interlock. Upon completion of the second panel level, the crown of the structure—defined by the apex vertices and upper panel edges—exhibited the highest degree of geometric irregularity. The vertical difference between the most outwardly tilted vertices measured 32 cm, which corresponded closely with predictions from the digital model. Using a laser gyroscope, the vertical inaccuracies relative to the reference geometry were determined to be under 4 mm, well within the permissible error margin of 10 mm.

3.3.Further panels levels

With the commencement of the third dome level assembly, the increasing inclination of cantilevered panels necessitated the introduction of temporary supporting struts. A central reinforced concrete pedestal served this purpose. Its placement can be seen in figure 5. The monolithic element was topped with a scaled-down model of the upper four dome levels. Threaded sockets were embedded at the geometric centers of the model's panel surfaces to anchor the struts. This scaled model was precisely located at the dome's focal point, and the orientation of the threads defined the directional vectors for strut deployment, providing targeted support for individual non-interlocked panels. From the third level onward, all elements required such temporary stabilization shown in figure 6 until the complete assembly was achieved, as the tilt-induced bending moments exceeded the tolerances of the joints.

Figure 5. research model before proceeding to assemble the second level of components.

All struts were fabricated as uniform-length components with limited telescopic extension capabilities. Before positioning any panel, a strut was first secured to the pedestal and directed toward the center of the intended panel, which was then rested atop it. Anti-slip pads ensured lateral stability during the simultaneous installation of surrounding panels. Each strut featured a calibrated scale along its outer surface, enabling precise adjustment during telescoping. When combined with deflection measurements following a predefined methodology (illustrated in accompanying diagrams), this allowed for high-accuracy evaluation of each panel's placement. The continued presence of previously

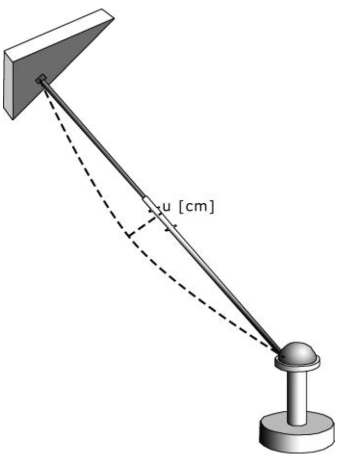

Figure 6. Diagram illustrating the use of support struts and deflection arrow measurement to assess panel placement inaccuracies

Table 1. Overview of support rod deflections during sequential panel installation. A steady trend indicating changes in the global stiffness of the structure is evident

57	58	59	60	61	62	63	64	65	66	67	68	69	70	71	72	73	74	75	76	77	78	79	80	81	
4,1	3,9	3,9	3,9	3,9	3,9	3,9	3,9	3,9	3,9	3,9	3,9	3,9	3,9	3,9	3,1	3,1	3,1	3,1	3,1	3,1	3,1	3,1	3,1	3,1	57
	2,15	2,1	2,05	2	1,95	1,95	1,95	1,9	1,9	1,9	1,9	1,9	1,9	1,9	1,85	1,85	1,85	1,85	1,85	1,85	1,85	1,85	1,85	1,85	58
		1,9	1,9	1,9	1,9	1,9	1,9	1,9	1,9	1,9	1,8	1,8	1,8	1,8	1,8	1,8	1,8	1,8	1,8	1,8	1,8	1,8	1,8	1,8	59
			1,6	1,6	1,6	1,6	1,6	1,6	1,6	1,6	1,6	1,6	1,6	1,6	1,55	1,55	1,55	1,55	1,55	1,55	1,55	1,55	1,4	1,4	60
				2,1	1,9	1,9	1,9	1,9	1,9	1,9	1,9	1,9	1,9	1,9	1,9	1,9	1,9	1,9	1,9	1,9	1,9	1,8	1,8	1,8	61
					0,3	0,3	0,3	0,3	0,3	0,3	0,3	0,3	0,3	0,3	0,3	0,3	0,25	0,25	0,25	0,25	0,25	0,25	0,25	0,25	62
						2,7	2,2	2,2	2,2	2,2	2,2	2,2	2,2	2,2	2,2	2,2	2,2	0,3	0,3	0,3	0,3	0,3	0,3	0,3	63
							3,3	3,3	3,3	3,3	3,3	3,3	3,3	3,3	3,3	3,3	3,3	3,3	3,3	3,3	3,1	3,1	3,1	3,1	64
								5,4	3,2	3,2	3,2	3,2	3,2	3,2	3,2	3,2	3,2	3,2	3	3	3	3	3	3	65
									0,5	0,5	0,5	0,5	0,5	0,5	0,5	0,5	0,5	0,5	0,5	0,5	0,5	0,5	0,5	0,3	66
										6,1	6,1	6,1	6,1	6,1	6,1	6,1	6,1	3,8	3,8	2,5	2,5	2,5	2,5	2,4	67
											4,6	4,6	4,6	4,6	4,6	4,6	2,7	2,7	2,7	2,7	2,7	2,7	2,7	1,2	68
												7,2	7,2	7,2	7,2	7,2	7,2	7,2	7,2	7,2	2,4	2,4	2,4	2,3	69
													4,6	4,6	4,3	4,3	4,3	4,3	4,3	4,3	4,3	2,9	2,9	2,9	70
														5,2	5,2	4,6	4,6	4,6	4,3	4,3	4,3	4,3	4,3	4,3	71
															6,1	6	6	6	5,7	5,8	5,4	5,3	5,3	5,1	72
																5	4,8	4,8	4,7	4,7	4,7	4,7	4,5	4,5	73
																	5,1	5	4,8	4,8	4,8	4,8	4,8	4,8	74
																		3,1	3,1	3	3	2,9	2,9	2,9	75
																			2,1	2,1	2	2	1,9	1,95	76
																				4	4	3,95	3,7	3,7	77
																					5,1	5	4,95	4,95	78
																						3,1	3	3	79
																							2,95	2,9	80
																								0,3	81

installed struts during subsequent placements enabled cumulative error tracking and the development of a time-sequenced deformation history, providing valuable insights into the evolving stiffness of the structure Whole values history is shown in table 1. As the panels lacked integrated threaded sockets, the struts terminated in steel plates with anti-slip matting to ensure secure panel contact. Each strut introduced a bending moment into the pedestal core, which necessitated a symmetrical, alternating installation sequence across opposing dome quadrants to prevent stress concentrations or torsional effects on the vertical axis of the pedestal. Similarly, a carefully orchestrated strut removal sequence was required to maintain equilibrium during de-shoring. The central pedestal was cast as a heavy-duty reinforced concrete element, intended for repeated use in various dome assembly applications.

During final installation of the uppermost levels, the strut extensions were dynamically adjusted to deflect previously installed panels and create sufficient clearance for new modules. The maximum panel translation reached 58 mm and was recorded at panel no. 95, necessitating the temporary displacement of panels no. 85 and 90. Upon completion of the full dome assembly, all joints were re-evaluated using a feeler gauge from both internal and external surfaces. The maximum permissible misalignments at this stage measured 0.9 mm on the interior and 1.3 mm externally. The discrepancy is attributed to enhanced mutual bearing action between panels, leading to smaller internal gaps due to increased inter-panel compression.

3.4. Skylight

The dome structure exhibits exceptionally high airtightness, with fully opaque panels devoid of any integrated glazing. To ensure the admission of natural light into the interior while simultaneously enabling stack ventilation, a light rose system was proposed at the dome's apex. This feature, composed of five modular elements, was designed to regulate interior environmental conditions through automated operability. The custom-fabricated triangular window frames were constructed with robust aluminum profiles, reaching a thickness of 14 cm. A circumferential industrial-grade sealing gasket was initially applied; however, post-installation performance evaluation revealed its insufficiency in achieving the required airtightness under variable pressure conditions. Each module followed a distinct mounting scheme, which necessitated the development of a dedicated anchoring strategy for secure attachment directly onto the dome panels. The glazing system itself comprised three layers of laminated glass. Due to fabrication-stage testing requirements, the inert gas within the interlayers had to be released, and the remaining installation was conducted in a depressurized state. Once the light rose modules were installed atop the dome, a comprehensive visual inspection of the entire structure was conducted to assess the integration quality, surface uniformity, and the performance of the sealing interfaces.

4.Panel signing system

The dome structure was designed for repeated assembly and disassembly, necessitating a clear, simple, and rapid system for the identification of all structural elements. The triangular panels existed in three dimensional variants, and due to their varying levels of wear and use across structural tiers, precise positional tracking was essential. A comprehensive marking system was developed, serving both as an assembly guide and a sequencing protocol for the entire construction process. Each panel was uniquely labeled to indicate its corresponding level within the structure, spatial orientation, and adjacent panels. Labels also included the panel type from the three previously mentioned panel types varying on their edge length and with data about directional cues for installation. This information was consolidated into a graphic format using a deformed topological map of the dome, maintaining spatial relationships between elements. The dataset enabled efficient grouping by levels or sections and facilitated pre-positioning of panels at the assembly site. It also allowed preparatory adjustment of inclination and

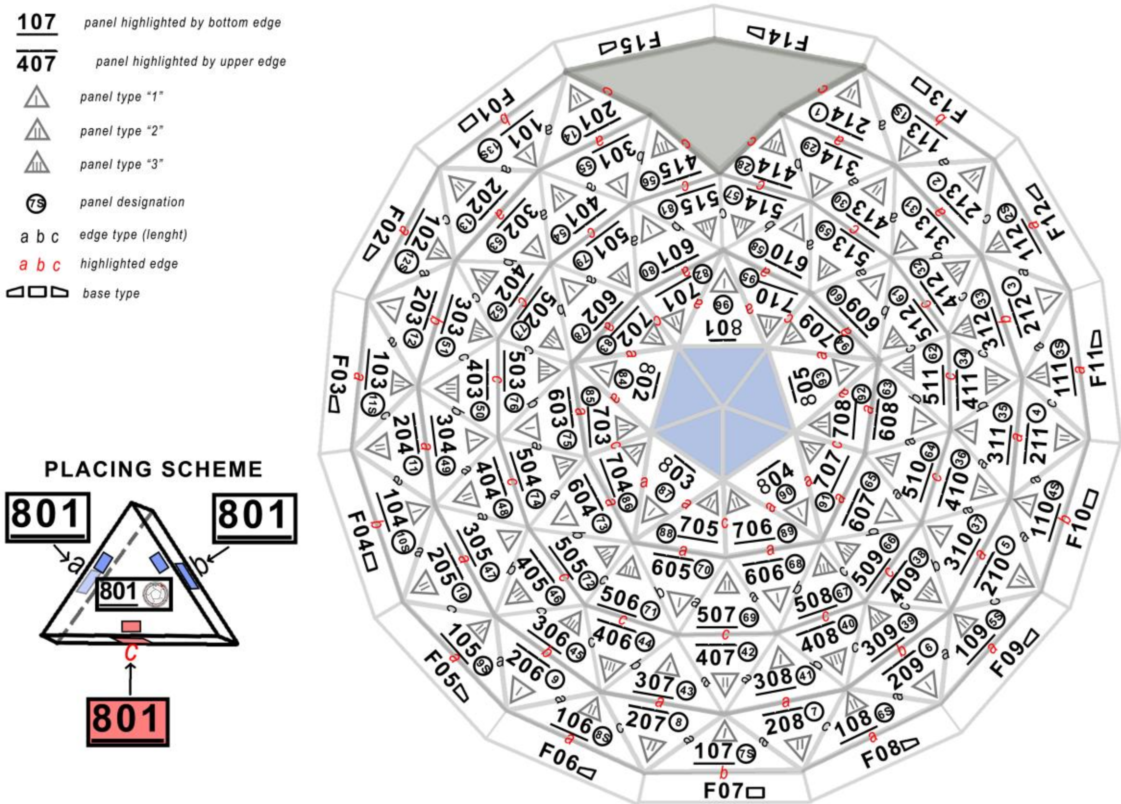

Figure 7. Panel marking system for unambiguous identification during assembly.

rotation angles on the aforementioned tilting platform prior to hoisting. The diagram illustrates the method of assembling the elements, clearly presenting the panelization of the entire structure, divided into five successive sequences composed of repeating module arrangements forming a regular icosahedron.

The system ensured consistent reassembly, minimizing structural wear and improving the fit of modules. Maintaining identical positioning of all elements across repeated assemblies reduced bending moments in the joints, leading to more uniform load distribution and extended durability of the structure. Provisional solutions—such as handwritten marking of adjoining edges—were replaced by durable metal identification plates affixed to the angle profiles of each panel. These plates displayed the neighboring element's number, its spatial orientation relative to the base, and a color-coded indication of the panel's primary edge. The primary edge marking facilitated rapid orientation of each element, indicating which edge to align with the vertical axis and whether the edge should face upward or downward. This provided six codable configurations per panel—sufficient for full identification during manual or automated assembly. Prior to implementing the identification system, four incorrect placements of panels occurred—three were immediately corrected, while one necessitated panel removal. Once deployed, the system enabled strict sequencing and supported potential automation of the assembly process. A detailed assembly manual was developed, independent of panel placement at the construction site. Using a camera-based identification system, the system could generate a real-time assembly sequence for each panel. By comparing current orientation with the target position, the system calculated necessary movements for accurate placement and simultaneously identified the subsequent required element. Compared to a full unmarked test assembly of the dome, the implementation of the identification system reduced the number of placement errors to zero and shortened the total assembly time from three weeks to two.

5. Endoscope inspection

Following the assembly and initial load testing of the structure, an internal inspection of the panels was conducted to evaluate wear, assess the visual integrity of steel-to-concrete joints at the edges, and observe joint behavior under load. Additionally, both inner surfaces of the panels were examined to identify any material degradation that could expose reinforcement or indicate discontinuities in the concrete matrix.

Each triangular panel, equipped with three tongues and three grooves at its corners, featured an inspection port designed for evaluating the internal mechanical connector. These ports provided access to a spacer pocket that isolates the connection from dust and contaminants within the internal cavity between the panel’s concrete layers. However, this method of inspection proved impractical for full-scale evaluation due to its labor-intensive nature and the time required to assess every connection. Nonetheless, it was sufficient for condition assessment of a representative sample of joints.

Using real-time photographs and video documentation, the condition of 42 connections was analyzed. Among them, only one required corrective action due to an inadequately engaged threaded connection. The visual data enabled assessment of weld integrity, steel component condition, movement allowances, and the quality of the concrete-to-steel interface. All joints exhibited appropriate protective treatment; however, minor corrosion was noted on several auxiliary screws securing the hybrid steel-concrete contact points—this is visible in Figure 8.

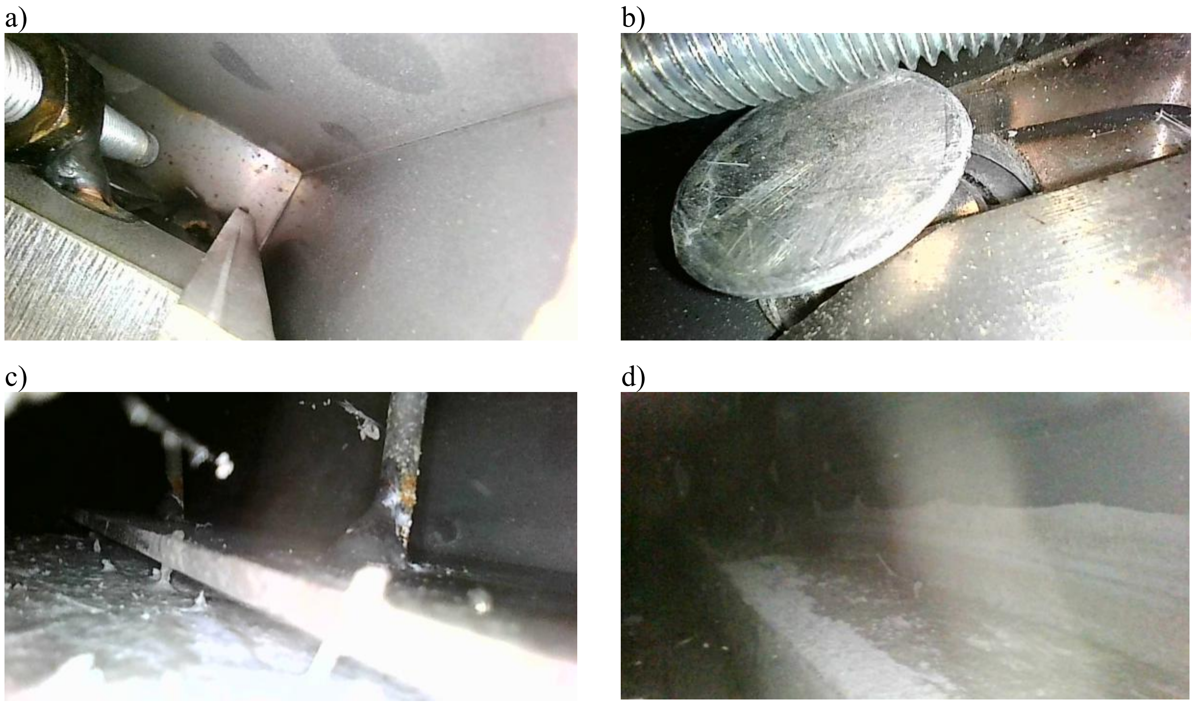

a) b) c) d)

Figure. 8 Endoscopic images captured during post-assembly inspection:
a) Sliding guide rail of the locking pin responsible for inter-panel mechanical engagement.
b) Locking pin of a panel enabling mutual interlocking between adjacent elements.
c) Prototype adhesive joint used in an earlier panel version, not tested under embedded structural conditions.
d) Interface between steel and GRC (Glass Reinforced Concrete) at the thickened lateral edge of the panel.

7. After assembly

The dome structure was completed in the autumn of 2024. Since that time, continuous monitoring has been conducted to assess deflections and joint gaps resulting from variable load conditions. Throughout the entire observation period up to May 2025, no exceedance of permissible deflection limits was recorded, and neither local nor global structural failures occurred. The panel-to-base connections were also systematically monitored. Only one instance of foundation disturbance was observed, where localized subsidence of the ground beneath a single panel led to tensile stresses in the dome structure. This temporary asymmetry affected the uniform load distribution, but no permanent damage or failure was reported. Except for this isolated case, the structure maintained a purely compressive stress regime. This behavior enhanced the load-bearing capacity by promoting joint sealing through compression and generating more ideal plate-like load transfer conditions. Furthermore, the dome's geometry—with its focal point located at a height of 1.75 meters—effectively minimized horizontal thrust forces. As a result, there was no need for specialized foundation design or subsoil reinforcement to counteract radial expansion forces, simplifying the substructure requirements.

Conclusions

The structure underwent multiple assembly and disassembly cycles to confirm the disassemblability of the test model. The first complete assembly process, conducted under controlled indoor conditions, confirmed the structure's ability to be fully assembled. The scope of the assembly tests also included horizontal load testing, simulating the lateral forces that would occur during standard use of the structure. Multiple assembly and disassembly cycles of the tested panels showed no signs of degradation, supporting further analysis of the system’s potential for repeated reuse of all its components.

Figure 9. Assembled dome at testing site prepared for initial loading for stiffness analysis.

The study describes the assembly challenges of a geodesic dome model with a structural behavior characteristic of a shell. It presents the difficulties encountered at all stages of the process—from conceptual design, through fabrication of components, selection of connection methods and materials, to assembly issues—and outlines the solutions applied. Following the assumed chronology of the test model's development, the paper details the errors, fabrication requirements, and their impact on the performance of the structure that has been shown in Figure 9. The effectiveness of the implemented spatial system and the validity of the initial modeling assumptions were confirmed.

References

[1] W. Bober, *Inside Out Outside In: Budowanie mostów pomiędzy sztuką a humanistyką, wiedzą a technologią*. Kraków: Księgarnia Akademicka, 2020.

[2] W. Bober and P. Stobiecki, "Experimental geodesic dome with a sandwich panels structure," in *Human Interaction & Emerging Technologies (IHIET-AI 2022): Artificial Intelligence & Future Applications*, 2022. doi: 10.54941/ahfe100896.

[3] T. Laila, A. Arruda, J. Barbosa, and E. Moura, "The constructive advantages of buckminster fuller's geodesic domes and their relationship to the built environment ergonomics," in *Advances in Intelligent Systems and Computing*, 2018. doi: 10.1007/978-3-319-60582-1_36.

[4] W. Bober, "Eksperymentalna powłoka żelbetowa," *Teka Komisji Architektury, Urbanistyki i Studiów Krajobrazowych*, vol. 12, no. 4, 1970, doi: 10.35784/teka.1528.

[5] A. Kaveh and S. Talatahari, "Geometry and topology optimization of geodesic domes using charged system search," *Structural and Multidisciplinary Optimization*, vol. 43, no. 2, 2011, doi: 10.1007/s00158-010-0566-y.

[6] H. Y. Chu, "The Evolution of the Fuller Geodesic Dome: From Black Mountain to Drop City," *Design and Culture*, vol. 10, no. 2, 2018, doi: 10.1080/17547075.2018.1466228.

[7] M. de Lózar de la Viña, "Domo house in carbondale, Illinois. R. B. Fuller, 1960," *ARQ*, no. 84, 2013, doi: 10.4067/S0717-69962013000200003.

[8] P. Shakor, "Glass Fibre Reinforced Concrete Use in Construction Related papers," *International Journal of Technology And Engineering System(IJTES)*, vol. 2, no. 2, 2011.